Journal of Advances in Modeling Earth Systems

RESEARCH ARTICLE
10.1029/2018MS001291

Key Points:
- A salt plume parameterization for the Arctic Ocean has been implemented into the AWI Climate Model
- The salt plume parameterization leads to simultaneous increase of sea ice (volume and concentration) and decrease of sea surface salinity in the Arctic
- It is argued that the salt plume parameterization alters the interplay between the atmosphere and the ocean in the Nordic Seas

Correspondence to:
D. Sidorenko,
dmitry.sidorenko@awi.de

Citation:
Sidorenko, D., Koldunov, N. V., Wang, Q., Danilov, S., Goessling, H. F., Gurses, O., et al. (2018). Influence of a salt plume parameterization in a coupled climate model. *Journal of Advances in Modeling Earth Systems*, *10*, 2357–2373. https://doi.org/10.1029/2018MS001291

Received 1 FEB 2018
Accepted 24 AUG 2018
Accepted article online 3 SEP 2018
Published online 27 SEP 2018

Influence of a Salt Plume Parameterization in a Coupled Climate Model

D. Sidorenko[1], N. V. Koldunov[1,2], Q. Wang[1], S. Danilov[1,3,4], H. F. Goessling[1], O. Gurses[1], P. Scholz[1], D. V. Sein[1,5], E. Volodin[6], C. Wekerle[1], and T. Jung[1,7]

[1]Alfred-Wegener-Institut Helmholtz-Zentrum für Polar- und Meeresforschung, Bremerhaven, Germany, [2]MARUM—Center for Marine Environmental Sciences, Bremen, Germany, [3]Department of Mathematics and Logistics, Jacobs University, Bremen, Germany, [4]A. M. Obukhov Institute of Atmospheric Physics Russian Academy of Science, Moscow, Russia, [5]Russian Academy of Science, Shirshov Institute of Oceanology, Moscow, Russia, [6]Russian Academy of Science, Institute of Numerical Mathematics, Moscow, Russia, [7]Institute of Environmental Physics, University of Bremen, Bremen, Germany

Abstract Sea ice formation is accompanied by the rejection of salt which in nature tends to be mixed vertically by the formation of convective plumes. Here we analyze the influence of a salt plume parameterization in an atmosphere-sea ice-ocean model. Two 330-yearlong simulations have been conducted with the AWI Climate Model. In the reference simulation, the rejected salt in the Arctic Ocean is added to the uppermost ocean layer. This approach is commonly used in climate modeling. In another experiment, employing salt plume parameterization, the rejected salt is vertically redistributed within the mixed layer based on a power law profile that mimics the penetration of salt plumes. We discuss the effects of this redistribution on the simulated mean state and on atmosphere–ocean linkages associated with the intensity of deepwater formation. We find that the salt plume parameterization leads to simultaneous increase of sea ice (volume and concentration) and decrease of sea surface salinity in the Arctic. The salt plume parameterization considerably alters the interplay between the atmosphere and the ocean in the Nordic Seas. The parameterization modifies the ocean ventilation; however, resulting changes in temperature and salinity largely compensate each other in terms of density so that the overturning circulation is not significantly affected.

Plain Language Summary The process of salt rejection during the sea ice formation is not properly parameterized in the climate models. Here we implement the salt plume parameterization in an atmosphere-ice-ocean model and analyze its influence on the simulated mean state and associated atmosphere–ocean linkages. Salt plume parameterization leads to simultaneous increase of sea ice (volume and concentration) and decrease of sea surface salinity in the Arctic. It is argued that salt plume parameterization alters the interplay between the atmosphere and the ocean in the Nordic Seas.

1. Introduction

Global climate change is manifested in the Arctic in phenomena such as the retreat of Arctic sea ice and Arctic amplification, that is, stronger warming of the Arctic compared to the rest of the globe. Questions related to the linkages of the polar climate with lower latitudes are drawing considerable attention of the scientific community (e.g., Jung et al., 2016). The ability of the research community to learn about possible future of Arctic climate relies largely on numerical climate models which are the main tools for exploring underlying processes, possible trends, and uncertainties. The Arctic Ocean, storing warm Atlantic water shielded from the atmosphere by a fresh and cold mixed layer residing above the halocline, is of particular interest in this context. Recent evidence for an "Atlantification" of the Arctic reveals the vulnerability of the present ocean state to the ongoing changes in the climate system (Polyakov et al., 2017). However, the ocean components of climate models, assessed either in ocean-only simulations (Ilıcak et al., 2016; Wang et al., 2016a, 2016b) or in coupled simulations such as those of the Climate Model Intercomparison Project (see, e.g., Pithan et al., 2014, Sgubin et al., 2017), show substantial shortcomings in simulating a realistic ocean state. Common model biases in ocean models are attributed to insufficient spatial resolution and shortcomings of parameterizations that aim to capture unresolved processes (Delworth et al., 2012; Scaife et al., 2011; Sein et al., 2017; Sterl et al., 2012; Wang et al., 2018; Wekerle et al., 2017; Zhang & Steele, 2007).

One of the important processes in the polar oceans is the rejection of salt during sea ice formation and the resulting formation of convective plumes that, at large, define properties of the mixed layer and the vertical

salinity structure (Nguyen et al., 2009). These processes act on small scales and cannot be explicitly resolved by global ocean models. It has been demonstrated previously that the use of a salt plume parameterization (SPP), which redistributes the rejected salt vertically, without triggering excessive mixing, considerably improves the simulated vertical structure of the upper ocean in standalone (Barthélemy et al., 2015; Jin et al., 2012; Nguyen et al., 2009) and coupled (Duffy et al., 1999, Bentsen et al., 2013) models. However, the way it influences the coupled climate system remains unclear. Since the inclusion of a salt plume parameterization changes the freshwater balance in the upper layers, it may affect the ocean well beyond the Arctic, but the extent of this impact is not known. In this study, we explore the long-term signal from using SPP in the AWI-CM (AWI Climate Model; Sidorenko et al., 2015, Rackow et al., 2016) based on 330-yearlong integrations under constant preindustrial climate forcing. We identify the impact of the parameterization on climate including associated changes in atmosphere–ocean linkages.

The next section briefly describes the SPP. This is followed by a description of the model setup in section 3. The main results are reported in section 4 and conclusions are provided in section 5.

2. SPP

In the course of the preparation of AWI-CM for Climate Model Intercomparison Project version 6, several preindustrial climate simulations using different parameter sets have been carried out under prescribed radiative conditions of 1850. Particular attention was paid to the changes in surface hydrography and sea ice between simulations in the Arctic Ocean as it is one of the key regions in studies conducted with AWI-CM. Changes in sea ice thickness could be achieved through modifying the so-called lead closing parameter, which determines the thickness of newly formed sea ice. Setting this parameter to smaller or larger values results in thinner or thicker sea ice, respectively, in agreement with other studies (e.g., Hutter et al., 2018). Furthermore, increasing the salinity of sea ice to 10 psu (from the default 5 psu) resulted in minor sea surface salinity (SSS) changes in the Arctic with nearly no change in the sea ice. The uniqueness of SPP among other tuning parameters (parameterizations) in the ocean is that it increases the sea ice (volume and concentration) and reduces SSS simultaneously.

Most ocean models add the salt that is rejected during sea ice formation to the uppermost ocean layer. In nature the rejected salt does not stay at the ocean surface but forms so-called salt plumes, which penetrate down to the bottom of the mixed layer and spread laterally (e.g., Duffy et al., 1999; Duffy & Caldeira, 1997; Nguyen et al., 2009). When the salt plume penetration is not accounted for, the vertical mixing scheme reacts to the decreased static stability of the upper water column and therefore may potentially destroy the upper pycnocline (see, e.g., discussion by Nguyen et al., 2009). For this reason, the inclusion of SPP is a step toward better model physics. However, as it will be shown below, inclusion of SPP has a tremendous effect on the simulated surface hydrography. Overall, therefore, it is important to examine the impact of SPP onto the simulated climate and associated atmosphere–ocean linkages in more detail.

Figure 2 (top left panel) shows the departure of the SSS, simulated with the AWI-CM without SPP, from the Polar Science Center Hydrographic Climatology (PHC, Steele et al., 2001). We use this difference to climatology only as rough measure of the model state given that PHC does not necessarily represent the preindustrial climate. The substantial SSS reduction obtained by applying the SPP in AWI-CM is shown in Figure 2 (top right panel). At the same time, the SSS difference to the climatology has not changed significantly over the rest of the globe (not shown).

SPP has been previously applied for the purpose of SSS bias reduction in ocean (see, e.g., Nguyen et al., 2009) and climate (see, e.g., Bentsen et al., 2013) models. However, the way how it is implemented varies between different models. Bentsen et al. (2013) evenly distribute the rejected salt down to the mixed layer depth which is defined as a density contrast of 0.4 kg/m^3 compared to the surface and is limited by 500 m. Nguyen et al. (2009) suggest to use a power law profile for salt distribution and define the mixed layer depth using a threshold on vertical density gradient. In this manuscript, we pursue the latter approach and leave the question on possible differences between schemes to another study.

In the following, we provide a detailed description of the model setups and analyze how the SPP affects the climate characteristics and atmosphere–ocean linkages in the Arctic and North Atlantic beyond the changes of the SSS.

3. Model Setup

In this study, we use the climate model AWI-CM (Sidorenko et al., 2015; Rackow et al., 2016). Its ocean-sea ice component is the unstructured-mesh Finite Element Sea Ice-Ocean Model (FESOM, Danilov et al., 2015; Wang et al., 2014). In this work it is configured on a mesh with resolution varying from nominal 1° in the interior of the ocean to 1/3° in the equatorial belt and 24 km north of 50°N (see Figure 1). The ocean surface is discretized with about 127,000 grid points, and 46 vertical levels are used. The time step is set to 30 min. This ocean-sea ice configuration has been used previously in the Coordinated Ocean-ice Reference Experiments phase II (CORE II), revealing that the results of FESOM on this mesh are well within the range of other well-established ocean models (see, e.g., Danabasoglu et al., 2014, 2016; Griffies et al., 2014; Wang et al., 2016a, 2016b).

The atmosphere is simulated with ECHAM6.3 (Stevens et al., 2013) in a setup with the T63 spectral resolution and 47 vertical levels. The time step is 450 s and the ocean–atmosphere coupling frequency is hourly to account for the diurnal cycle.

AWI-CM was spun up for 300 years under constant preindustrial forcing from 1850. The spin-up run was started from ocean and sea ice initial conditions obtained from the output of a stand-alone ocean run under CORE II atmospheric forcing for the years 1948–2007. The SPP was switched off in FESOM during the stand-alone run as well as during the subsequent coupled spin-up. We then continued with two simulations of 330 years each, which are different only in the treatment of salt rejected during sea ice formation.

In the reference simulation (hereafter referred to as ***ref***), the salt rejected during ice formation is added to the uppermost ocean grid cell as in most existing state-of-the-art climate models. In the second simulation (hereafter referred to as ***spp***, lowercase), the formation of salt plumes is parameterized as suggested by Nguyen et al. (2009): the rejected salt is added to the mixed layer and distributed vertically according to a power law profile ($n = 5$; see Figure S1). The bottom of the mixed layer is determined by a vertical density gradient threshold of 0.01 kg/m^3.

4. Results

4.1. Ocean Response

During the process of sea ice formation, the rejected salt in *ref* is accumulated at the surface, reducing the static stability of the upper water column. This leads to convection, which is manifested by enlarged vertical mixing coefficients (a value of 0.005 m^2/s is used in our experiments). As a result, the rejected salt is uniformly mixed within the upper mixed layer. In contrast, the main effect of SPP is to redistribute the rejected salt to the bottom of the mixed layer without incurring vertical mixing. Thus, the near-surface water in *spp* is considerably fresher than in *ref* (see Figure 2, top panel). The accompanying change in the sea surface temperature (SST) is illustrated in Figure 2 (bottom panel). A reduction in SST by ~0.2 °C is found in the Barents, Greenland-Iceland-Norwegian (GIN), and Labrador Seas. A warming by ~0.2 °C is found along the path of the North Atlantic Current and south of the Bering Strait. The SST over the central Arctic is slightly increased (by ~0.018 °C over the ice covered area in response to an increased freezing temperature associated with the reduced SSS). In agreement with these differences, *spp* simulates up to ~30 cm thicker sea ice in winter (January-February-March) along the ice edge (see Figure 5, right panel).

One can expect that the export of more buoyant surface waters from the Arctic basin potentially reduces the deepwater formation in the northern North Atlantic and GIN Seas. Indeed, an average reduction by ~500 m in the maximum mixed layer depth (MLD; diagnosed as the depth where the potential density exceeds the surface density by 0.125 kg/m^3) is clearly seen in Figure 3. A pronounced decrease in MLD is found everywhere north of Iceland, which is the strongest over the GIN Seas. In the Central Arctic Ocean the MLD has decreased from ~60 to ~30 m. In the Labrador Sea (LS), there is a small MLD decrease along the path of the West Greenland Current accompanied by a slight increase toward the interior of the LS and around the southeastern part of Greenland.

For the central Arctic, the results agree with the findings by Jin et al. (2012), who used the ocean-sea ice components of CESM without air-sea feedback. They report on the reduction in the simulated SSS and MLD when

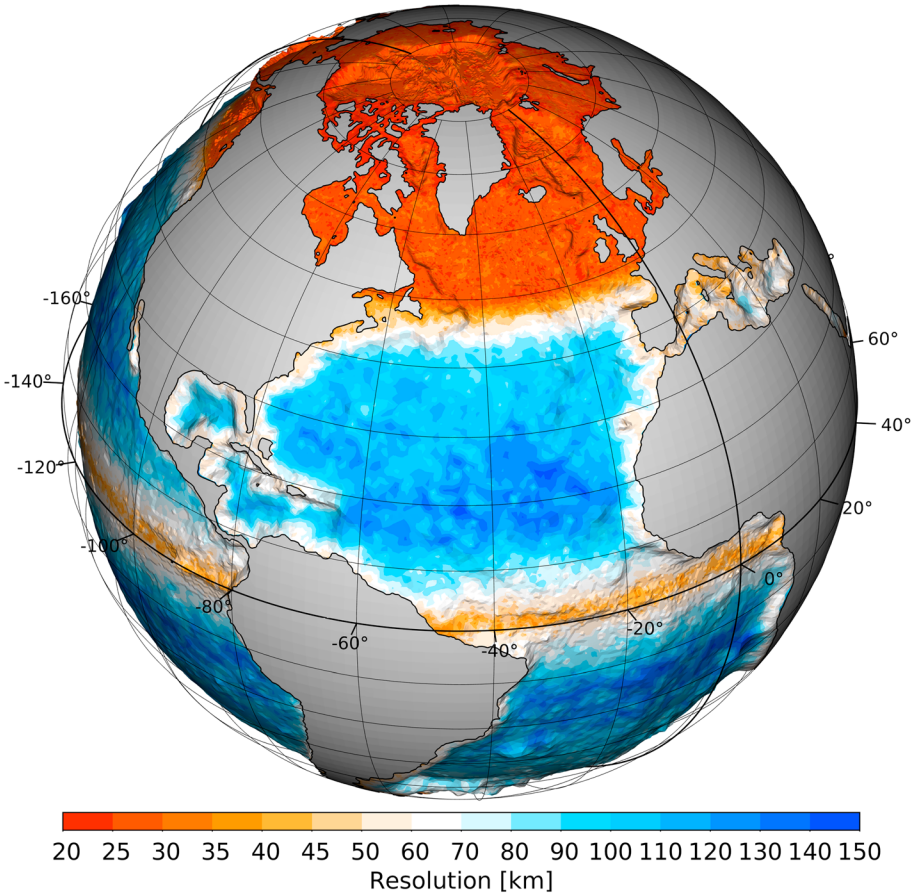

Figure 1. Mesh resolution (in km) used in the sea ice-ocean component of the coupled climate model.

using SPP, which improved the agreement between the model and the CTD profile data collected around the Beaufort Gyre.

The variability of the MLD annual maximum in the LS and GIN Seas is shown in Figure 4. The mean MLD over the LS does not change significantly. In the GIN Seas, the maximum MLD drops from ~1,900 m in *ref* to ~1,000 m in *spp* within the first 100 years. Thereafter, the significant difference in MLD persists throughout the simulation. The strength of the MLD variability is largely unchanged in both the LS and GIN Seas.

Changes in the deep convection have two essential implications for the climate. First, they modify the deep-water ventilation via air-sea interaction and thus potentially the thermohaline circulation. Second, they control the amount of heat supplied to the atmosphere from the ocean interior at high latitudes, which can directly impact the atmospheric circulation. In the following, we analyze the change in the air-sea interaction induced by the SPP via modifications in deepwater formation regions.

4.2. Air-Sea Interaction

The amount of heat which can be supplied to the atmosphere by the ocean is strongly constrained by the thickness of the oceanic mixed layer. In the response to atmospheric cooling of the ocean surface, in particular in winter, oceanic convection acts to increase the surface temperatures of the ocean. The heat from the upper ocean is then released to the atmosphere, which can cause, among others, atmospheric convection. A decrease in the ocean MLD corresponds to a reduction of heat lost by the ocean to the atmosphere. Because low-level heating through the ocean can affect the atmospheric circulation, variations in the strength of the ocean deep convection have been linked with the large-scale atmospheric circulation patterns, as reflected for example by sea level pressure (SLP; see also Gerdes et al., 2013).

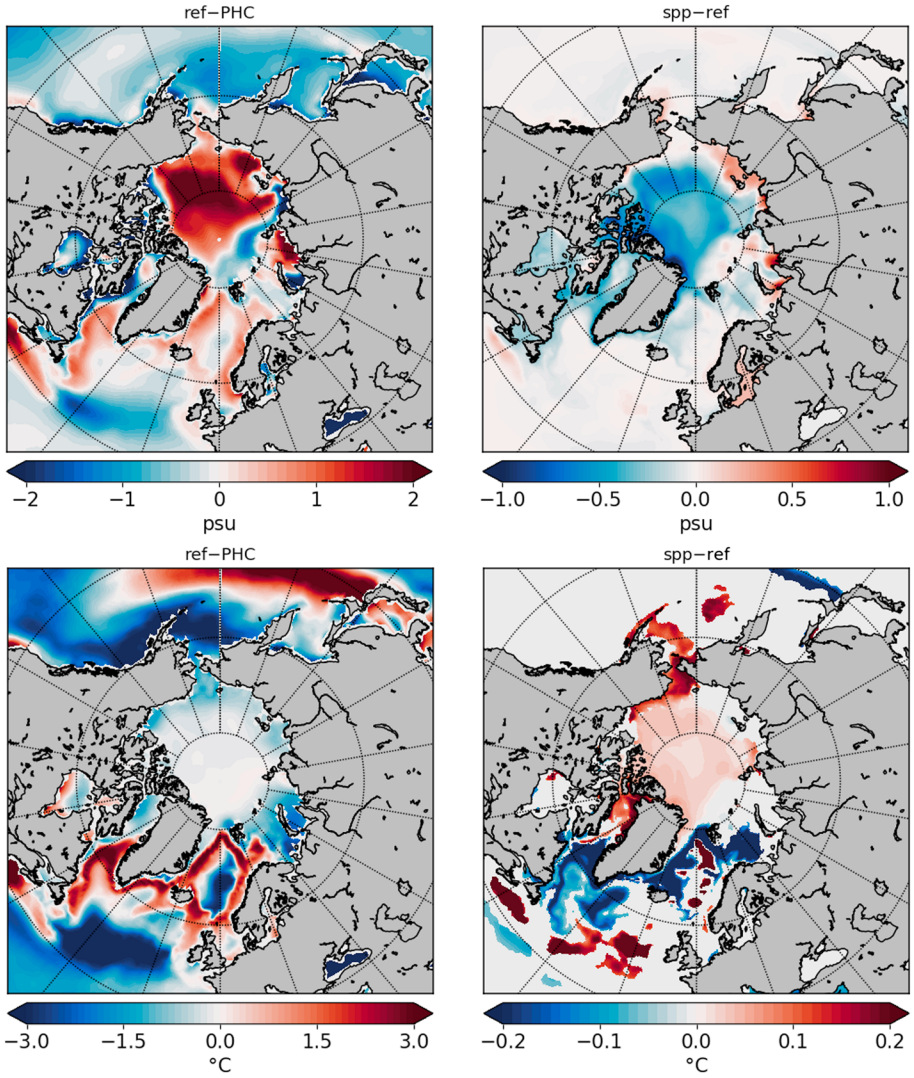

Figure 2. (top row) The departure of sea-surface salinity (SSS) from PHC 2.1 climatology for (left) *ref* and (right) the difference between *spp* and *ref*, averaged over the years 100–330. Only statistically significant differences (p value <0.05) are shown. (bottom row) The same but for sea surface temperature (SST).

4.2.1. Deep Convection in the Labrador Sea

Differences between composite patterns of SLP anomalies computed for the periods of high ($dMLD^+$) and low ($dMLD^-$) values of MLD in the Labrador Sea (LS-MLD patterns of variability) are shown in the left panel of Figure 6. Events where the MLD deviates from the mean by more than one standard deviation have been considered. The spatial structure of the SLP patterns resembles that of the Arctic Oscillation (AO; first EOF of SLP in the Northern Hemisphere; not shown). The LS mode in *ref* is very similar to that in *spp* as indicated by the difference between respective patterns (bottom panel in Figure 6). The difference between the winter (January-February-March) mean SLP in *ref* and *spp* (left plot in Figure 5) shows a tripolar structure with centers over Europe, the central Arctic, and the Aleutians.

The corresponding patterns of the LS-MLD mode for atmospheric January-February-March surface air temperature (SAT) are shown in Figure 6 (middle panel). The phases of $dMLD^+$ are associated with stronger land–sea SAT gradients around the Labrador Sea, supporting increased generation of cyclones which bring warm air to the central Arctic. Consequently, the $dMLD^+$ phase in the Arctic is characterized by higher SAT and simultaneously decreased SLP there while the opposite holds for the $dMLD^-$ phases. The LS-MLD patterns for SAT change only slightly between the runs with and without salt plume parameterization

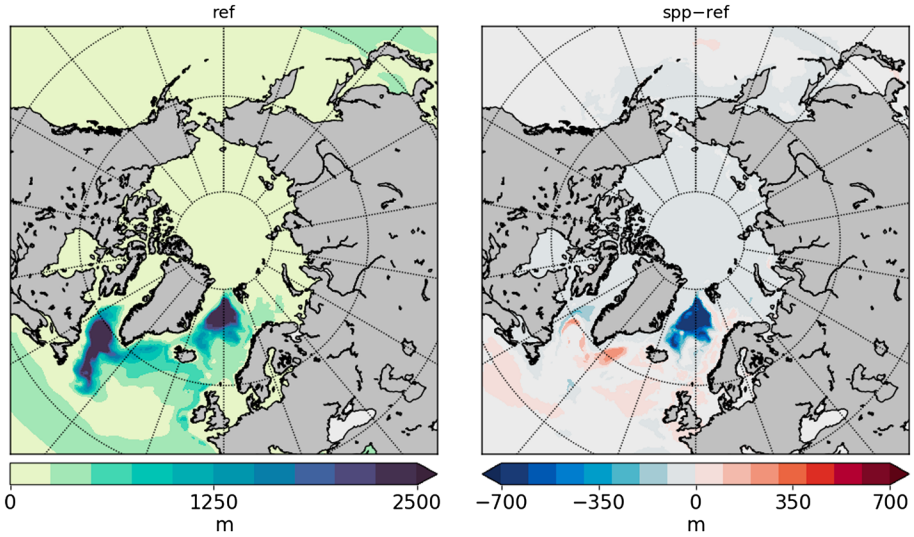

Figure 3. (left) Annual maximum mixed layer depth (MLD) in ref, averaged over years 100–330 and (right) the difference in MLD between spp and ref. Only statistically significant differences (p value <0.05) are shown.

(Figure 6, bottom middle panel). The SAT pattern along the ice edge in the Barents and GIN Seas is stronger in *spp* and agrees with the drop of the SLP over this area.

The respective LS-MLD patterns for sea ice thickness (last column in Figure 6) are characterized by an Eurasia-America dipole as a response to the surface winds being more cyclonic (anticyclonic) during $dMLD^+$ ($dMLD^-$). The difference between the two runs in the Arctic Ocean depicts a strong positive anomaly, which is in agreement with the reduced SAT (bottom middle panel in the same figure). Furthermore, as indicated by Deser et al. (2000) and thereafter by Gerdes et al. (2013), $dMLD^+$ phases are associated with sea ice extending farther into the LS despite its isolating effect on the heat exchange between ocean and atmosphere. In the *spp* run this effect is even more pronounced than in the *ref* run, supporting the shift of the MLD toward the interior of the LS (see Figure 3).

Overall, the air-sea interaction associated with the convective regimes in the Labrador Sea is only marginally modified by SPP. This is not surprising in view of the fact that the MLD maximum in the LS shows a similar behavior between the runs (Figure 4, top panel).

4.2.2. Deep Convection in the GIN Seas

The composite differences related to GIN-MLD fluctuations are shown in Figure 7. The SLP composites resemble a dipole through $dMLD^+$ and $dMLD^-$ phases. The amplitude of this atmosphere–ocean connection is smaller than that associated with the LS (note the difference in color bars between Figures 6 and 7). In contrast to *ref*, the GIN-MLD pattern in *spp* is characterized by a more meridionally aligned dipole pattern. Moreover, the pan-Arctic anomaly is the largest signal distinguishing $dMLD^+$ and $dMLD^-$ phases (left column in Figure 7). Related patterns for SAT (middle column in Figure 7) show the largest difference in the Barents and Nordic Seas. Opposite to *ref* the *spp* is characterized by warmer and colder air temperatures during $dMLD^+$ and $dMLD^-$ over GIN and Barents Seas, respectively. The answer lies in the more persistent sea ice cover in *spp* in the GIN and Barents Seas which is absent in *ref* (see Figures S2 and S3). In contrast to *ref*, $dMLD^+$ ($dMLD^-$) events in *spp* are distinguished by different ice cover regimes (no sea ice/sea ice). In no sea ice regime, any air temperature below the ocean SST may lead to the deepwater formation, and conversely, the convection will be blocked if the sea ice is present. Also note that in *ref* more cold air is advected to the GIN seas from the Arctic during $dMLD^+$ phases (SLP anomaly in the left column of Figure 7) while it is not the case in *spp* (more meridionally aligned SLP anomaly dipole) indicating the importance of the dynamical response.

Related ice thickness patterns are shown in Figure 7 (right column) and display major differences between *ref* and *spp*. In *ref*, they indicate more sea ice north of the GIN Seas main convection sites during $dMLD^+$ as compared to $dMLD^-$. This is consistent with the SAT patterns. Similar to the ice distribution patterns for the LS,

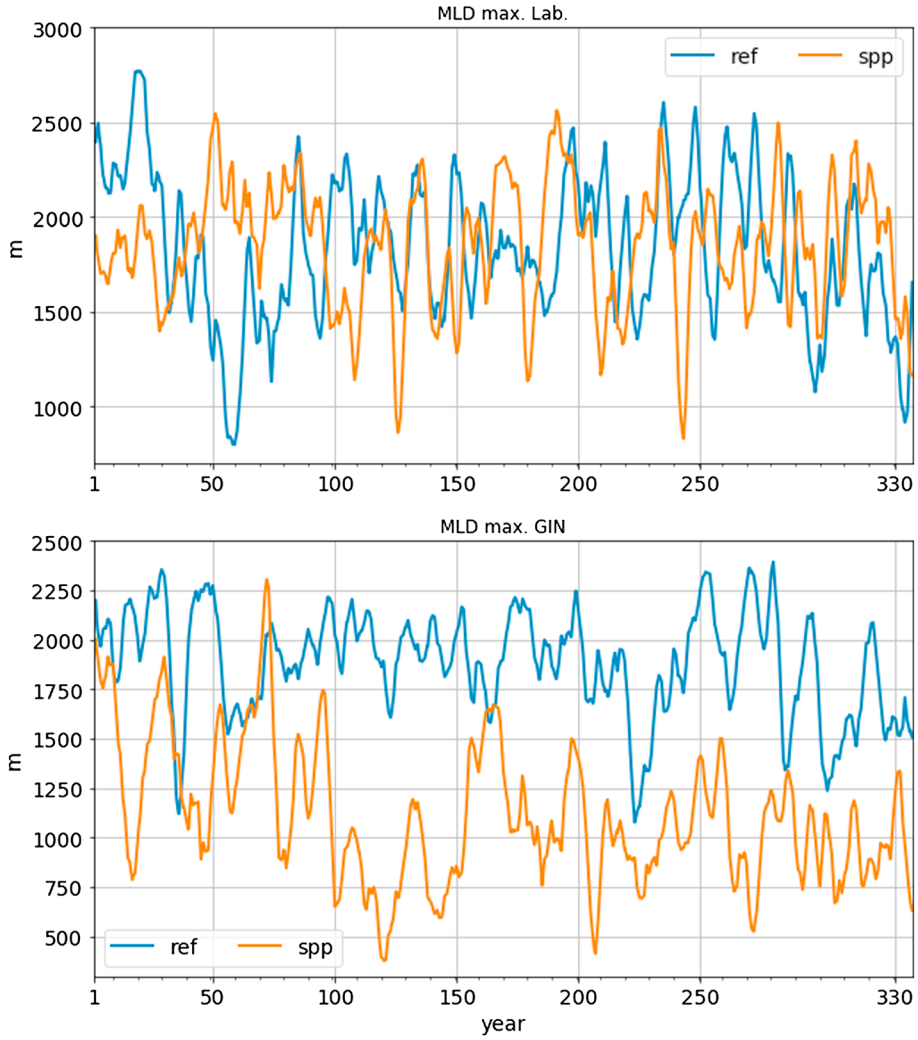

Figure 4. Time series for MLD annual maximum in the (top) Labrador and (bottom) GIN seas. A 5-year moving average filter has been used.

this finding agrees with Deser et al. (2000) and Gerdes et al. (2013). However, this signal is missing in the *spp* run. Moreover, only the *spp* run exhibits the occurrence of the Odden ice feature (see, e.g., Shuchman et al., 1998) during $dMLD^{-}$ phases, which stands in contrast to the findings reported in Gerdes et al. (2013). Indeed, as illustrated in Figure 3, the mean convective activity is strongly reduced in the GIN Seas through SPP,

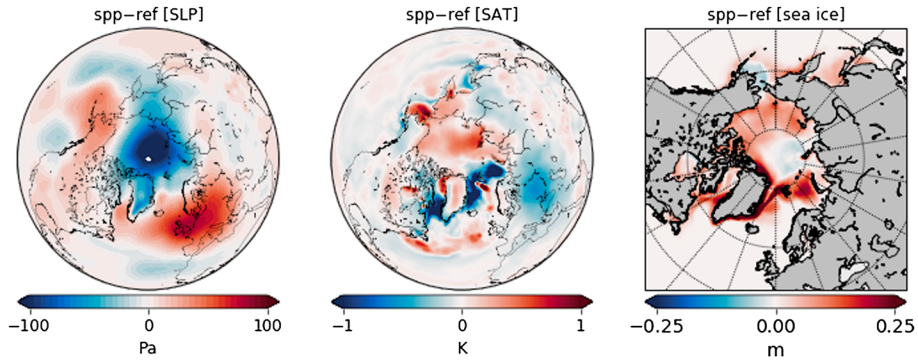

Figure 5. (left to right) (JFM) difference in sea level pressure (SLP), surface air temperature (SAT), and sea ice thickness between spp and ref.

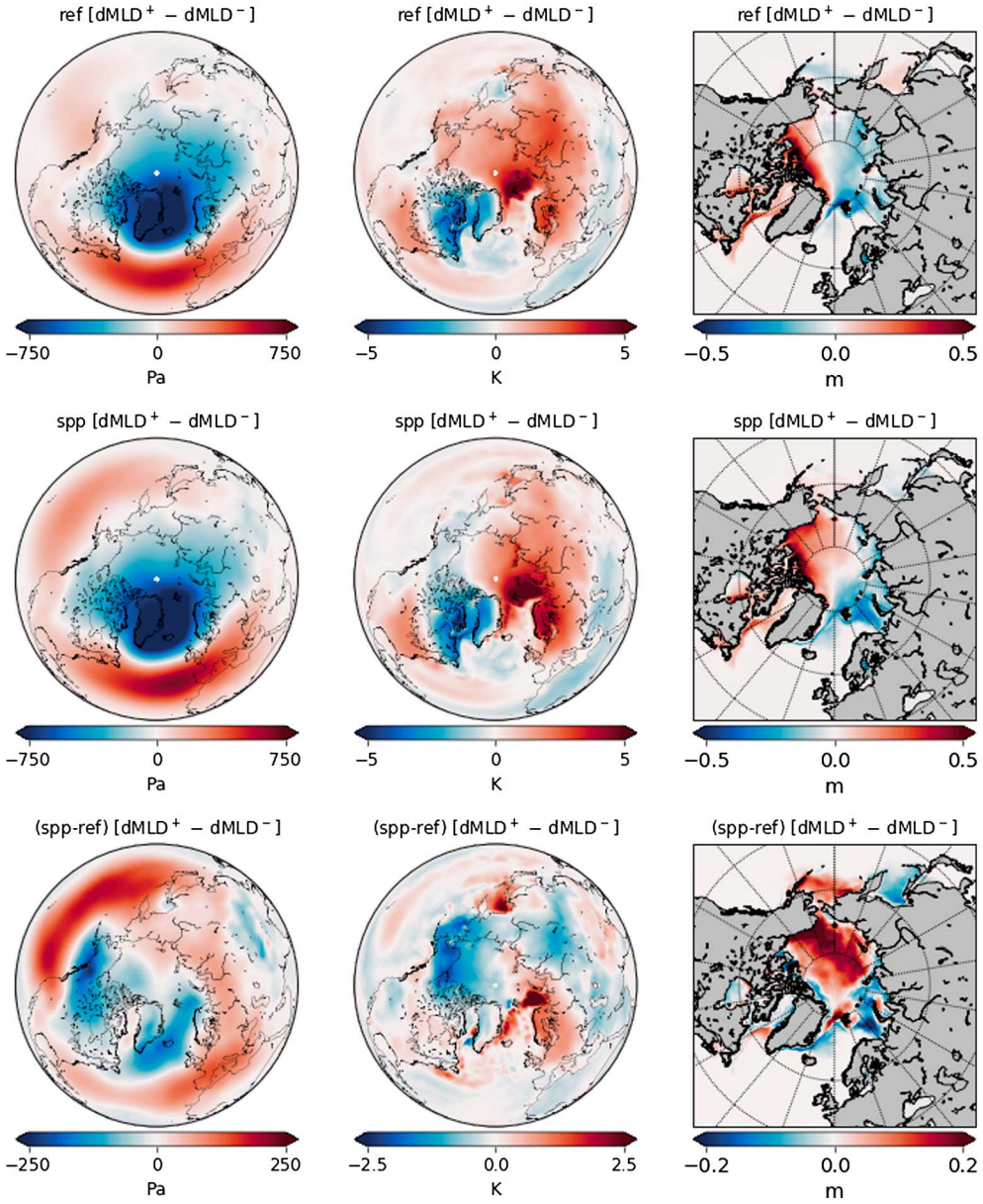

Figure 6. (top to bottom) Differences between composites for high and low mixed layer depth (MLD) events in the Labrador Sea shown for *ref*, *spp*, and the respective difference between the two runs (top minus middle plots). (left to right) Sea level pressure (SLP), surface air temperature (SAT), and sea ice thickness. Events where the MLD deviates from the mean by more than one standard deviation have been considered.

implying that the heat exchange between the ocean and the atmosphere is reduced in *spp*, and even more so during $dMLD^-$ phases, resulting in stronger sea ice formation. We conclude that the processes in the GIN and Barents Seas are considerably modified by SPP. Change in sea ice regimes there has been shown in literature to have a strong impact on the Arctic climate and cold winter extremes (e.g., Petoukhov & Semenov, 2010; Smedsrud et al., 2013).

4.3. Freshwater Transports and Surface Fluxes

Freshwater exports through main Arctic gates for both runs are shown in Figure 8. Through the Davis Strait the freshwater export in *ref* is ~103 mSv, which is reduced by ~6 mSv in *spp* mainly due to the change in the liquid constitute. At the same time, the freshwater export through the Fram Strait has

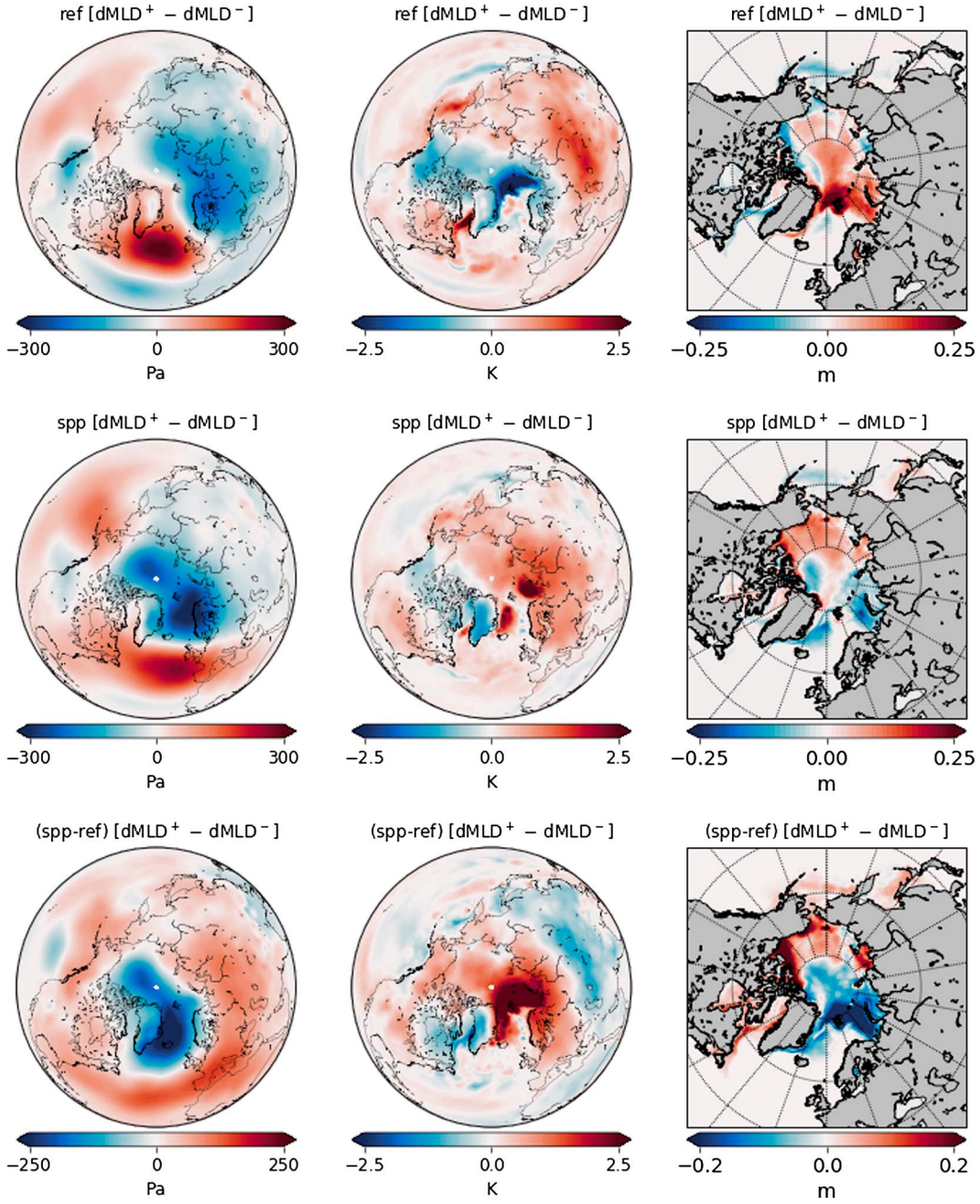

Figure 7. Same as in Figure 6 but for MLD events in the GIN seas.

increased by ~17 mSv (from 104 mSv in *ref*) due to the considerable change in its solid part. Concurrently, the combined import of freshwater through Barents Sea Opening (25 mSv in *ref*) and Bering Strait (93 mSv in *ref*) has been increased by only ~1 mSv. Averaged over 330 years the total freshwater export through the main gates in *spp* has increased by ~10 mSv compared to *ref* (Figure 9, top panel). This agrees with an averagely lower freshwater content in the Arctic Ocean in *spp* compared to *ref* (Figure 9, bottom panel). This is not surprising since SPP traps the rejected salt in the subsurface of the Arctic Ocean supporting the increase in export of liquid and solid freshwater at the surface through the Fram Strait to the Nordic Seas. The difference between *P-E* fluxes in two simulations is shown in Figure 10 and only modestly compensates for the difference in the total freshwater export. Augmented with the freshwater

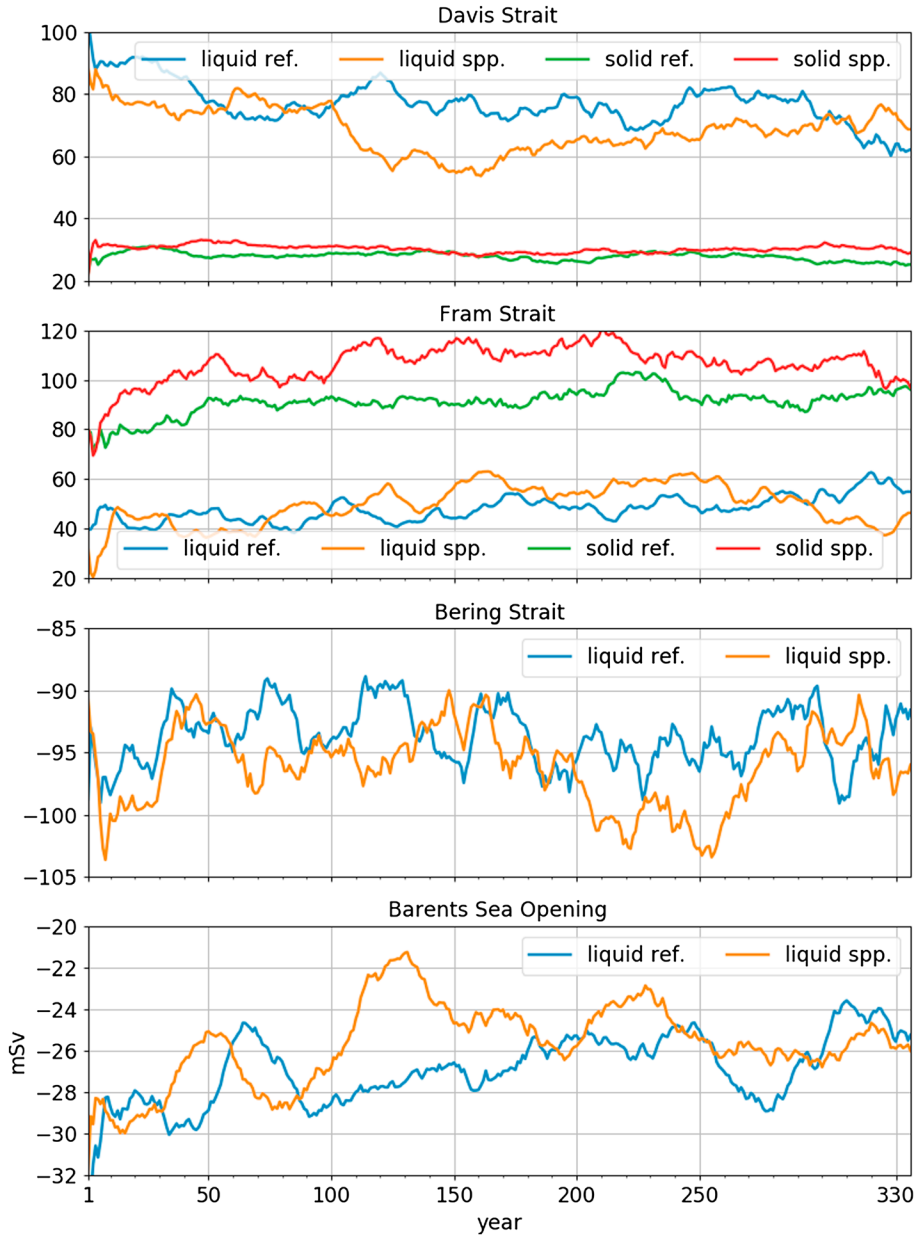

Figure 8. Freshwater transports across Arctic gates including liquid and solid constitutes. A 25-year moving average filter has been used.

flux from the ice growth (melt), we obtain the total freshwater flux applied to the ocean surface which is shown in Figure 11 (top left panel). The positive part of the differences (red color in the top right panel of Figure 11) in the Arctic Ocean and Nordic Seas corresponds primarily to more ice growth in the *spp* compared to *ref* and is applied to the ocean by virtue of the SPP scheme. The negative part comes primarily from the sea ice melt and is applied directly at the ocean surface. Apparently, increase in the upper vertical stratification of the Arctic Ocean in *spp* leads to more sea ice formation north of Svalbard, in the Greenland Sea, and slightly in the central Arctic. At the same time more melting occurs south of Svalbard, along the East Greenland pathways and along the ice edge in the Labrador Sea. Moreover, the presence of sea ice in GIN and Barents Seas in the *spp* run leads to more heat being kept in the ocean as illustrated in Figure 11 (bottom right panel), which shows the difference in the net heat fluxes at the ocean surface between two runs.

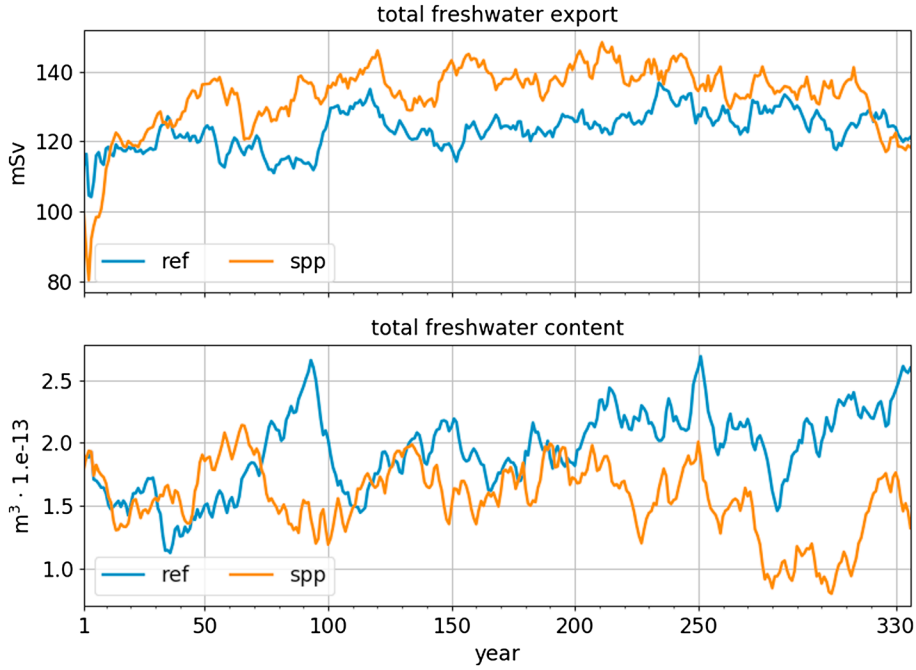

Figure 9. Total freshwater budget in the Arctic. A 25-year moving average filter has been used.

4.4. Ocean Hydrography

The difference in sea-surface dynamic height between the runs (not shown) is primarily explained by its steric constituent (SH; Figure 12, left panel) and reaches up to 3 cm in the Arctic due to temperature and salinity changes below the surface. The thermosteric and halosteric contributions separately (see Figure 14, middle and right panels) show even larger differences, implying that they partly compensate each other in terms of density. Although fresher at the surface, the *spp* simulates on average warmer and more saline waters in the Arctic water column as compared to *ref*. This is supported by the increased ice export from the Arctic Ocean (see Figure 8) and the heat being trapped there due to the increase in the sea ice cover. At the same

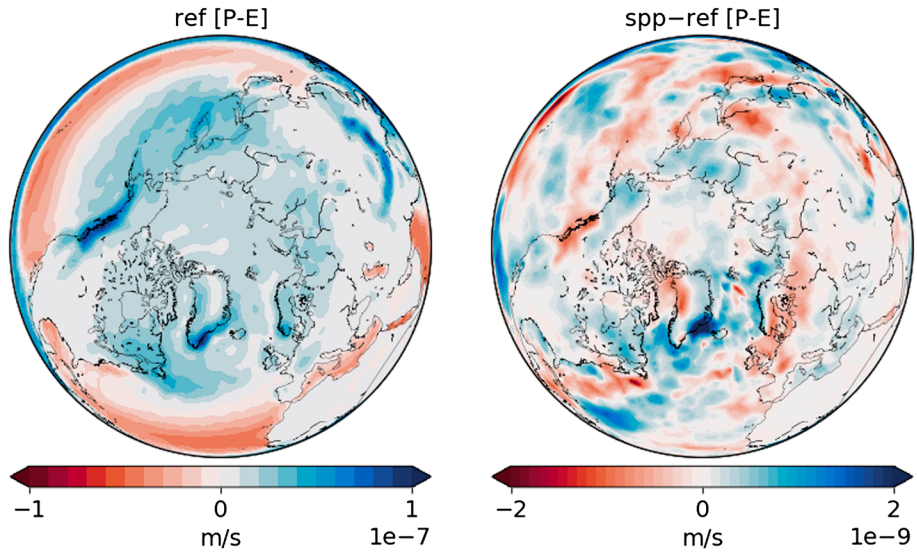

Figure 10. (top, left) P-E in *ref*, time mean over 330 years and (right) the difference in P-E. Note the change in the color bar range between plot.

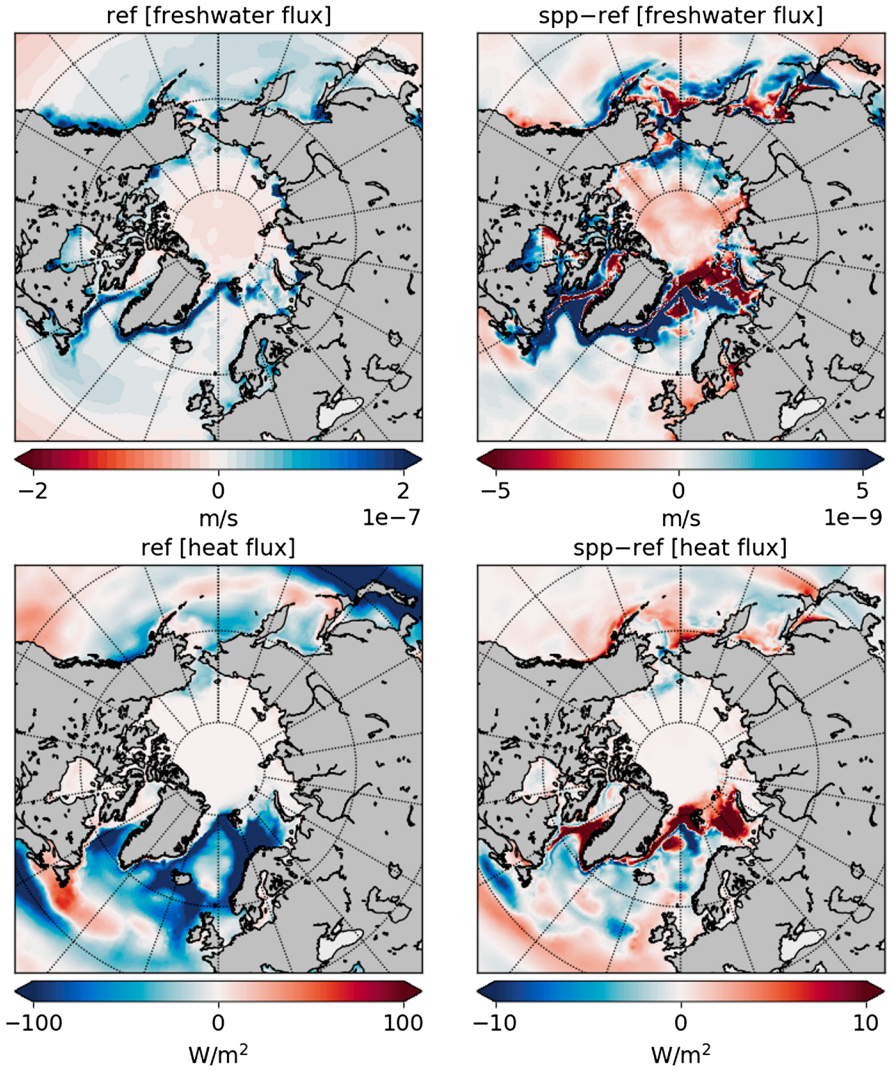

Figure 11. (top) Total surface freshwater flux (positive to the ocean) applied to the ocean in *ref* including the ice growth (melt) rate, time mean over 330 years (left), and the difference in freshwater flux between runs. Note that injection of salt due to ice formation in *spp* is instantaneously subtracted from the surface and redistributed within the MLD using the power law profile. (bottom) Same but for the total heat flux (positive to the ocean).

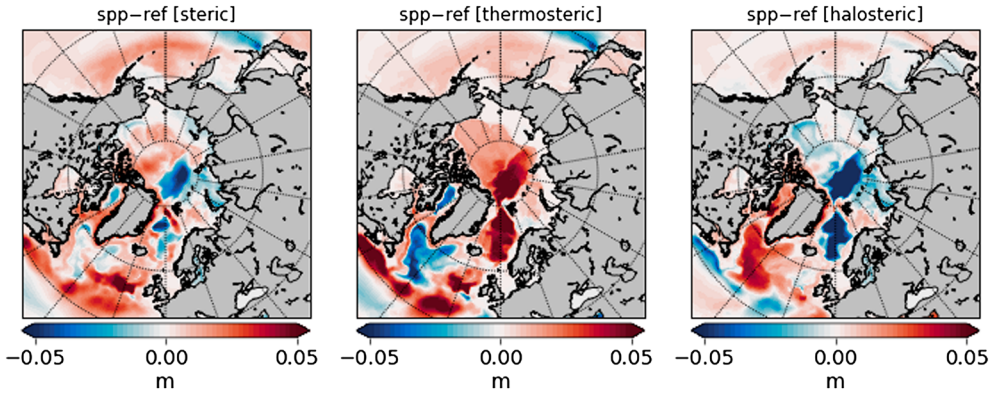

Figure 12. Differences in steric, thermosteric, and halosteric heights between model runs.

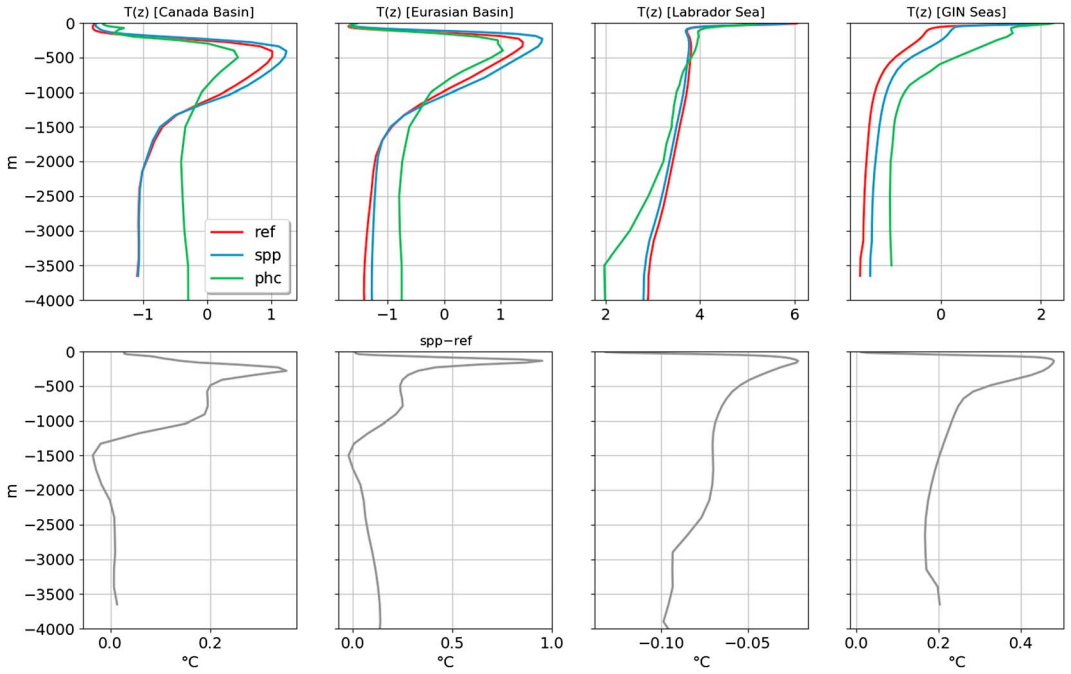

Figure 13. (top row) Temperature profiles in different basins averaged over the last 100 years (after ~700 years of integration of AWI-CM in total). Respective profiles from the PHC 2.1 climatology are shown in red. (bottom row) The difference between the model runs (spp minus ref).

time, waters in the LS are colder and fresher in *spp* as a consequence of increased freshwater export from the Arctic Ocean. The relative contributions to SH differences are such that the thermosteric component dominates in the Amerasian Basin and the halosteric one dominates in the Eurasian Basin of the Arctic Ocean. In the central LS, the thermosteric and halosteric contributions largely compensate each other.

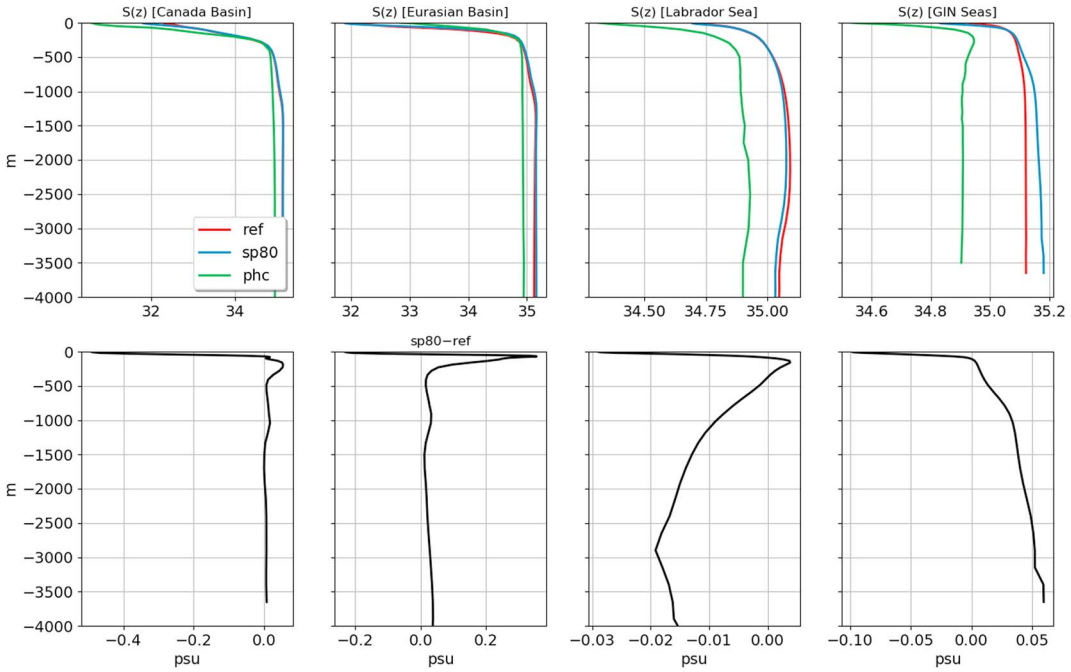

Figure 14. Same as in Figure 13 but for salinity.

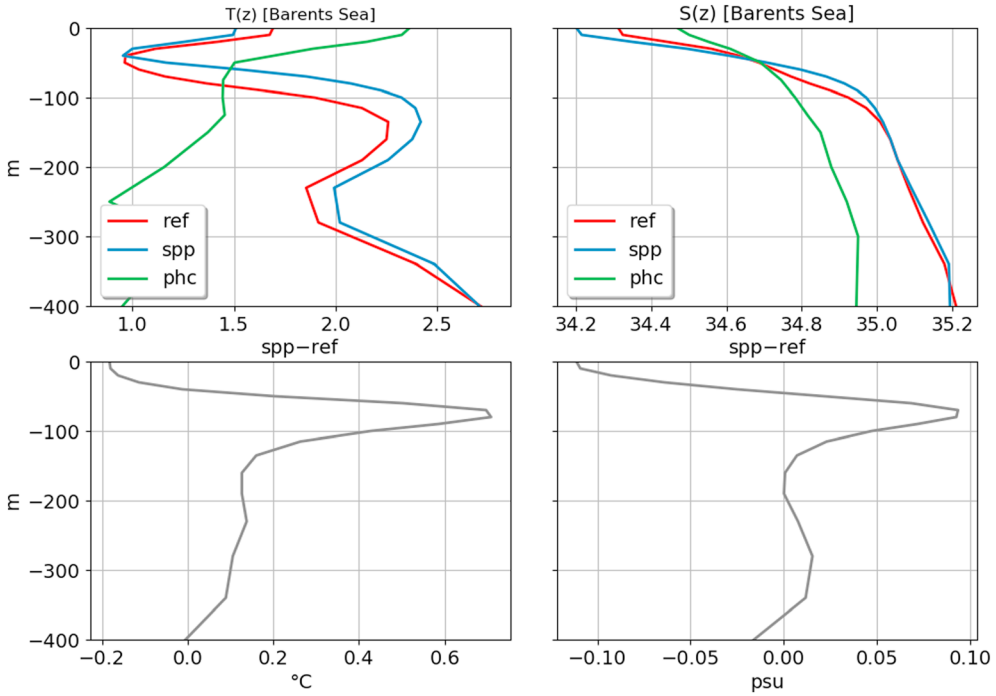

Figure 15. Same as in Figures 13 and 14 but shown for the Barents Sea separately.

To explore this in more detail, temperature and salinity profiles in four key basins are presented in Figures 13 and 14 and separately in Figure 15 for the Barents Sea. The differences between experiments are small compared to biases. In the Canada and Eurasian basins, both runs simulate too strong thermocline and too cold deep ocean compared to climatology. In the Canada basin, the steric difference between the *spp* and *ref* runs comes primarily from increased water temperatures in *spp* within the upper 1500 m, whereas the salinity difference remains small. The opposite behavior is seen in the Eurasian Basin, where the slightly increased salinity throughout the water column contributes more to the SH than the increase in temperature. Not much change is seen in the Labrador Sea, whereas in the GIN and Barents Seas the salinity and temperature profiles show positive differences complying with the difference in the surface heat (less heat lost from the ocean in *spp* compared to *ref*) and freshwater fluxes there. In the GIN seas the difference is persistent through the entire depth. There, the excessive heat and salt in the subsurface gradually penetrates deeper ocean via the vertical mixing and reaches the bottom. We speculate that this effect can be reduced by choosing more carefully the criteria for the MLD depth where SPP is applied and by choosing finer vertical resolution. Concurrently, the temperature and salinity profiles show positive differences in the Eurasian Basin. While the changes in surface hydrography are large, the deep ocean is changed only moderately, with the largest signal found in the GIN Seas. Yet differences in temperature and salinity largely compensate each other in terms of density. Hence, they only marginally impact the simulated thermohaline circulation and cause only a local effect onto GIN seas.

Indeed, we do not observe any significant changes in transport of Atlantic Water into the GIN Seas and transport of dense waters out through the Denmark Strait (see Figure S4). Hence, averaged over the whole time period, the difference in the Atlantic meridional overturning between the runs is less than 0.2 Sv (see Figure S5).

5. Summary and Conclusions

We have analyzed the effects, induced by a salt plume parameterization (SPP), on the simulated pre-industrial climate, including atmosphere–ocean linkages. The uniqueness of SPP among other tuning parameters (parameterizations) in the ocean is that it increases the sea ice (volume and concentration) and reduces SSS simultaneously. To this end, two simulations with the AWI Climate Model have been conducted. In the

simulation without salt plume parameterization (*ref*), the rejected salt is added to the uppermost ocean grid cell. This approach is commonly used in climate modeling. In the simulation with a salt plume parameterization (*spp*), the vertical salt penetration is parameterized as suggested by Nguyen et al. (2009). In *spp*, the simulated Arctic sea surface salinity (SSS) is reduced by ~0.5 psu compared to *ref*.

The *spp* run shows a systematic decrease in the MLD by ~500 m north of Iceland, with the strongest signal over the GIN Seas. The depth range of MLD change primarily affects the waters which are still too deep to pass the Denmark Strait with a maximum depth of 600 m. Hence, this decrease does not lead to changes in the AMOC. The signal is accompanied by a pan-Arctic increase in sea ice thickness by up to 30 cm in the vicinity of the Atlantic ice edge, in the Barents and Greenland Seas. In the Greenland Sea the latter is combined with the occurrence of the Odden sea ice feature, which is absent in *ref*. Only small changes are found in the Labrador Sea, where *spp* simulates a slight shift of the convective activity toward the interior of the Labrador Sea. At the same time, the amplitude of variability of the winter maximum MLD shows no significant changes between the runs in the GIN and Labrador Seas.

The impact of SPP on atmosphere–ocean linkages has been analyzed based on composite patterns of SLP, SAT, and sea ice thickness for periods of high ($dMLD^+$) and low ($dMLD^-$) values of the MLD in the GIN and Labrador Seas. The largest impact is found in the GIN Seas, where in *ref* deep convection is associated with colder (warmer) air temperatures over GIN and Barents Seas during $dMLD^+$ ($dMLD^-$) phases. This finding is consistent with earlier results from stand-alone ocean sea ice models (e.g., Gerdes et al., 2013). However, such behavior is absent in the *spp* run because the convective activity is highly suppressed there through the increase in the sea ice cover, implying that the heat exchange between the ocean and atmosphere becomes weaker during $dMLD^-$ phases. At the same time, *spp* exhibits a pattern of variability with warm (cold) temperatures over the Barents and Greenland Seas during $dMLD^+$ ($dMLD^-$) phases which is absent in *ref*.

The analysis of the freshwater budgets indicates an increased export of solid freshwater from the Arctic in *spp* compared to *ref*. This increase is primarily realized through the Fram Strait and is not compensated by changes in the surface buoyancy fluxes or through other Arctic gates. Concurrently, the freshwater content in the Arctic Ocean and GIN Seas is decreased in *spp*.

In the ocean hydrography, large changes take place not only in the surface salinity in the Arctic Ocean but also in the deep ocean in the GIN Seas and in the Atlantic water layer of the Arctic Ocean. Furthermore, changes in temperature and salinity largely compensate each other in terms of density and thus rarely affect the large-scale circulation including the Atlantic meridional overturning circulation.

In summary, the following chain of events is triggered by SPP in the Arctic Ocean and beyond:

1. Salt rejected during ice formation is transferred to the subsurface ocean layer, resulting in a negative SSS anomaly.
2. Due to the increased vertical stratification more sea ice is formed. Excessive solid freshwater melts while exported from the Arctic to the Labrador Sea along the Eastern Greenland pathways, creating a positive anomaly in the freshwater content there.
3. Salt left in the Arctic and in the GIN seas creates negative freshwater anomalies there which are further modified through ocean dynamics.
4. Heat is trapped in the Arctic Ocean and Nordic Seas through the increased sea ice cover and stronger halocline in the Barents Sea, around Svalbard, Baffin Bay, and along Eastern Greenland.
5. Heat and salt left in the subsurface gradually penetrates into the deeper ocean via vertical mixing and other mechanisms (see, e.g., Pemberton & Nilsson, 2016) reaching the bottom. We speculate that this effect can be modified by tuning the criteria for the MLD where SPP is applied or by changing the vertical resolution.

In summary, therefore, we conclude that salt plume parameterizations can lead to substantial changes in the simulated Arctic surface hydrography. Changes in the simulated mean climate and associated atmosphere–ocean linkages are rather moderate in general, although the interplay between the atmosphere and the ocean can be altered considerably in the GIN Seas. Our results suggest that a salt plume parameterization can be beneficial for climate simulations, and the AWI Climate Model is now using this parameterization by default, also in the upcoming Climate Model Intercomparison Project version 6 simulations.

Data Availability

Data sets related to this article can be found at https://swiftbrowser.dkrz.de/public/dkrz_035d8f6ff058403bb42f8302e6badfbc/Sidorenko_SPP_2018/.

Acknowledgments
The work described in this paper has received funding from the Helmholtz Climate Initiative REKLIM (Regional Climate Change; Q. Wang, D. Sidorenko), the ERA.Net RUS project NAtMAP (Amending North Atlantic Model Biases to Improve Arctic Prediction, BMBF grant 01DJ16003, and RFBR grant 16-55-76004 ERA_a; S. Danilov, H. Goessling, D. Sidorenko, E. Volodin), the APPLICATE (European Union's Horizon 2020 Research and Innovation programme grant agreement 727862; T. Jung), the FRAM (FRontiers in Arctic marine Monitoring program; C. Wekerle), the projects S1 and S2 of the Collaborative Research Centre TRR 181 *Energy Transfer in Atmosphere and Ocean* funded by the German Research Foundation (S. Danilov, N. Koldunov, P. Scholz), the PRIMAVERA (European Union's Horizon 2020 Research and Innovation programme grant agreement 641727), and the state assignment of FASO Russia theme 0149-2018-0014 (D. Sein). The simulations were performed at the North-German Supercomputing Alliance (HLRN).

References

Barthélemy, A., Fichefet, T., Goosse, H., & Madec, G. (2015). Modeling the interplay between sea ice formation and the oceanic mixed layer: Limitations of simple brine rejection parameterizations. *Ocean Modelling*, *86*, 141–152. https://doi.org/10.1016/j.ocemod.2014.12.009

Bentsen, M., Bethke, I., Debernard, J. B., Iversen, T., Kirkevåg, A., & Seland, Ø. (2013). The Norwegian Earth system model, NorESM1-M—Part 1: Description and basic evaluation of the physical climate. *Geoscientific Model Development*, *6*(3), 687–720. https://doi.org/10.5194/gmd-6-687-2013

Danabasoglu, G., Yeager, S. G., Bailey, D., Behrens, E., Bentsen, M., Bi, D., et al. (2014). North Atlantic simulations in coordinated ocean-ice reference experiments phase II (CORE-II). Part I: Mean states. *Ocean Modelling*, *73*, 76–107. https://doi.org/10.1016/j.ocemod.2013.10.005

Danabasoglu, G., Yeager, S. G., Kim, W. M., Behrens, E., Bentsen, M., Bi, D., et al. (2016). North Atlantic simulations in Coordinated Ocean-ice reference experiments phase II (CORE-II). Part II: Inter-annual to decadal variability. *Ocean Modelling*, *96*, 65–90. https://doi.org/10.1016/j.ocemod.2015.11.007

Danilov, S., Wang, Q., Timmermann, R., Iakovlev, N., Sidorenko, D., Kimmritz, M., et al. (2015). Finite-element sea ice model (FESIM), version 2. *Geoscientific Model Development*, *8*(6), 1747–1761. https://doi.org/10.5194/gmd-8-1747-2015

Delworth, T. L., Rosati, A., Anderson, W., Adcroft, A. J., Balaji, V., Benson, R., et al. (2012). Simulated climate and climate change in the GFDL CM2.5 high-resolution coupled climate model. *Journal of Climate*, *25*(8), 2755–2781. https://doi.org/10.1175/JCLI-D-11-00316.1

Deser, C., Walsh, J., & Timlin, M. (2000). Arctic sea ice variability in the context of recent atmospheric circulation trends. *Journal of Climate*, *13*(3), 617–633. https://doi.org/10.1175/1520-0442(2000)013<0617:ASIVIT>2.0.CO;2

Duffy, P. B., & Caldeira, K. (1997). Sensitivity of simulated salinity in a three-dimensional ocean model to upper ocean transport of salt from sea-ice formation. *Geophysical Research Letters*, *24*, 1323–1326. https://doi.org/10.1029/97GL01294

Duffy, P. B., Eby, M., & Weaver, A. J. (1999). Effects of sinking of salt rejected during formation of sea ice on results of an ocean-atmosphere-sea ice climate model. *Geophysical Research Letters*, *26*, 1739–1742. https://doi.org/10.1029/1999GL900286

Gerdes, R., Hurka, J., Karcher, M., Kauker, F., & Köberle, C. (2013). Simulated history of convection in the Greenland and Labrador seas, 1948–2001. *The Nordic Seas: An Integrated Perspective*, 221–238. https://doi.org/10.1029/158GM15

Griffies, S. M., Yin, J., Durack, P. J., Goddard, P., Bates, S. C., Behrens, E., et al. (2014). An assessment of global and regional sea level for years 1993–2007 in a suite of interannual CORE-II simulations. *Ocean Modelling*, *78*, 35–89. https://doi.org/10.1016/j.ocemod.2014.03.004

Hutter, N., Losch, M., & Menemenlis, D. (2018). Scaling properties of arctic sea ice deformation in a high-resolution viscous-plastic sea ice model and in satellite observations. *Journal of Geophysical Research: Oceans*, *123*, 672–687. https://doi.org/10.1002/2017JC013119

Ilıcak, M., Drange, H., Wang, Q., Gerdes, R., Aksenov, Y., Bailey, D., et al. (2016). An assessment of the Arctic Ocean in a suite of interannual CORE-II simulations. Part III: Hydrography and fluxes. *Ocean Modelling*, *100*, 141–161. https://doi.org/10.1016/j.ocemod.2016.02.004

Jin, M., Hutchings, J., Kawaguchi, Y., & Kikuchi, T. (2012). Ocean mixing with lead-dependent subgrid scale brine rejection parameterization in a climate model. *Journal of Ocean University of China*, *11*(4), 473–480. https://doi.org/10.1007/s11802-012-2094-4

Jung, T., Gordon, N. D., Bauer, P., Bromwich, D. H., Chevallier, M., Day, J. J., et al. (2016). Advancing polar prediction capabilities on daily to seasonal time scales. *Bulletin of the American Meteorological Society*, *97*(9), 1631–1647. https://doi.org/10.1175/BAMS-D-14-00246.1

Nguyen, A. T., Menemenlis, D., & Kwok, R. (2009). Improved modeling of the Arctic halocline with a subgrid-scale brine rejection parameterization. *Journal of Geophysical Research*, *114*, C11014. https://doi.org/10.1029/2008JC005121

Pemberton, P., & Nilsson, J. (2016). The response of the central Arctic Ocean stratification to freshwater perturbations. *Journal of Geophysical Research: Oceans*, *121*, 792–817. https://doi.org/10.1002/2015JC011003

Petoukhov, V., & Semenov, V. (2010). A link between reduced Barents-Kara Sea ice and cold winter extremes over northern continents. *Journal of Geophysical Research*, *115*, D21111. https://doi.org/10.1029/2009JD013568

Pithan, F., Medeiros, B., & Mauritsen, T. (2014). Mixed-phase clouds cause climate model biases in Arctic wintertime temperature inversions. *Climate Dynamics*, *43*(1–2), 289–303. https://doi.org/10.1007/s00382-013-1964-9

Polyakov, I. V., Pnyushkov, A. V., Alkire, M., Ashik, I. M., Baumann, T., Carmack, E. C., et al. (2017). Greater role for Atlantic inflows on sea-ice loss in the Eurasian Basin of the Arctic Ocean. *Science*, *356*(6335), 285–291. https://doi.org/10.1126/science.aai8204

Rackow, T., Goessling, H. F., Jung, T., Sidorenko, D., Semmler, T., Barbi, D., & Handorf, D. (2016). Towards multi-resolution global climate modeling with ECHAM6-FESOM. Part II: Climate variability. *Climate Dynamics*, *50*(7-8), 2369–2394. https://doi.org/10.1007/s00382-016-3192-6

Scaife, A. A., Copsey, D., Gordon, C., Harris, C., Hinton, T. J., Keeley, S. P., et al. (2011). Improved Atlantic winter blocking in a climate model. *Geophysical Research Letters*, *38*, L23703. https://doi.org/10.1029/2011GL049573

Sein, D. V., Koldunov, N. V., Danilov, S., Wang, Q., Sidorenko, D., Fast, I., et al. (2017). Ocean modeling on a mesh with resolution following the local Rossby radius. *Journal of Advances in Modeling Earth Systems*, *9*(7), 2601–2614. https://doi.org/10.1002/2017MS001099

Sgubin, G., Swingedouw, D., Drijfhout, S., Mary, Y., & Bennabi, A. (2017). Abrupt cooling over the North Atlantic in modern climate models. *Nature Communications*, *8*. https://doi.org/10.1038/ncomms14375

Shuchman, R. A., Josberger, E. G., Russel, C. A., Fischer, K. W., Johannessen, O. M., Johannessen, J., & Gloersen, P. (1998). Greenland Sea Odden Sea ice feature: Intra-annual and interannual variability. *Journal of Geophysical Research*, *103*, 12,709–12,724. https://doi.org/10.1029/98JC00375

Sidorenko, D., Rackow, T., Jung, T., Semmler, T., Barbi, D., Danilov, S., et al. (2015). Towards multi-resolution global climate modeling with ECHAM6–FESOM. Part I: Model formulation and mean climate. *Climate Dynamics*, *44*(3–4), 757–780. https://doi.org/10.1007/s00382-014-2290-6

Smedsrud, L. H., Esau, I., Ingvaldsen, R. B., Eldevik, T., Haugan, P. M., Li, C., et al. (2013). The role of the Barents Sea in the Arctic climate system. *Reviews of Geophysics*, *51*, 415–449. https://doi.org/10.1002/rog.20017

Steele, M., Morley, R., & Ermold, W. (2001). PHC: A global ocean hydrography with a high-quality Arctic Ocean. *Journal of Climate*, *14*(9), 2079–2087. https://doi.org/10.1175/1520-0442(2001)014<2079:PAGOHW>2.0.CO;2

Sterl, A., Bintanja, R., Brodeau, L., Gleeson, E., Koenigk, T., Schmith, T., et al. (2012). A look at the ocean in the EC-earth climate model. *Climate Dynamics*, *39*(11), 2631–2657. https://doi.org/10.1007/s00382-011-1239-2

Stevens, B., Giorgetta, M., Esch, M., Mauritsen, T., Crueger, T., Rast, S., et al. (2013). Atmospheric component of the MPI-M earth system model: ECHAM6. *Journal of Advances in Modeling Earth Systems*, *5*(2), 146–172. https://doi.org/10.1002/jame.20015

Wang, Q., Ilicak, M., Gerdes, R., Drange, H., Aksenov, Y., Bailey, D. A., et al. (2016a). An assessment of the Arctic Ocean in a suite of interannual CORE-II simulations. Part I: Sea ice and solid freshwater. *Ocean Modelling*, *99*, 110–132. https://doi.org/10.1016/j.ocemod.2015.12.008

Wang, Q., Ilicak, M., Gerdes, R., Drange, H., Aksenov, Y., Bailey, D. A., et al. (2016b). An assessment of the Arctic Ocean in a suite of interannual CORE-II simulations. Part II: Liquid freshwater. *Ocean Modelling*, *99*, 86–109. https://doi.org/10.1016/j.ocemod.2015.12.009

Wang, Q., Wekerle, C., Danilov, S., Wang, X., & Jung, T. (2018). A 4.5 km resolution Arctic Ocean simulation with the global multi-resolution model FESOM 1.4. *Geoscientific Model Development*, *11*, 1229–1255. https://doi.org/10.5194/gmd-11-1229-2018

Wang, Q., Danilov, S., Sidorenko, D., Timmermann, R., Wekerle, C., Wang, X., et al. (2014). The Finite Element Sea Ice-Ocean Model (FESOM) v.1.4: formulation of an ocean general circulation model. *Geoscientific Model Development*, *7*, 663–693. https://doi.org/10.5194/gmd-7-663-2014

Wekerle, C., Wang, Q., Danilov, S., Schourup-Kristensen, V., von Appen, W. J., & Jung, T. (2017). Atlantic water in the Nordic seas: Locally eddy-permitting ocean simulation in a global setup. *Journal of Geophysical Research: Oceans*, *122*, 914–940. https://doi.org/10.1002/2016JC012121

Zhang, J., & Steele, M. (2007). Effect of vertical mixing on the Atlantic water layer circulation in the Arctic Ocean. *Journal of Geophysical Research*, *112*, C04S04. https://doi.org/10.1029/2006JC003732